Available online at www.sciencedirect.com
SCIENCE DIRECT®
ELSEVIER
Nuclear Instruments and Methods in Physics Research A 521 (2004) 512–529
NUCLEAR INSTRUMENTS & METHODS IN PHYSICS RESEARCH Section A
www.elsevier.com/locate/nima

LIBO—a linac-booster for protontherapy: construction and tests of a prototype

U. Amaldi[a,*,1], P. Berra[a], K. Crandall[a], D. Toet[a], M. Weiss[a], R. Zennaro[a], E. Rosso[b], B. Szeless[b], M. Vretenar[b], C. Cicardi[c,d], C. De Martinis[c,d], D. Giove[c,d], D. Davino[e,f], M.R. Masullo[e,f], V. Vaccaro[e,f]

[a] *TERA Foundation, Via Puccini 11, 28100 Novara, Italy*
[b] *CERN, Geneva 23, Switzerland*
[c] *Department of Physics, Università degli Studi di Milan, Italy*
[d] *INFN Section of Milano, Via F.lli Cervi 201, 20090 Segrate, Italy*
[e] *Department of Physics, University Federico II of Naples, Italy*
[f] *INFN Section of Naples, Complesso Univ. MSA, Via Cinthia, 80126 Napoli, Italy*

Received 10 July 2003; accepted 15 July 2003

Abstract

LIBO is a proton accelerator that operates at 3 GHz, the same frequency as the one adopted in the about 7500 electron linacs used for radiotherapy all over the world. Such a high frequency was chosen to obtain a large gradient (on average more than 10 MV/m), and thus a short linac (about 15 m) to boost the energy of the protons, extracted at about 60 MeV from a cyclotron, up to the 200 MeV needed for the treatment of deep-seated tumours.

This paper describes the design study of the full 3 GHz Side Coupled Linac (modular structure, nine modules) and the construction and tests of the LIBO prototype (first module), which was built to accelerate protons from 62 to 74 MeV with an RF peak power of 4.4 MW. The items discussed are the beam dynamics parameters of the module (longitudinal and transverse acceptances), the constructional elements and procedures, the accuracies of the various mechanical elements, the cooling system, the RF tuning, the RF measurement and the RF power tests. These tests showed that, after a short conditioning time, the gradient in each of the four tanks of the module could reach 28.5 MV/m, much larger than the nominal project value (15.8 MV/m). The last section of the paper describes the successful acceleration tests performed at the Laboratori Nazionali del Sud of INFN in Catania with a solid-state 3 GHz modulator lent by IBA.

PACS: 87.56.−v

Keywords: Linac; Energy booster; Proton therapy; SCL

1. Global status of protontherapy

About 7500 linacs, accelerating electrons to energies in the range from 5 to 25 MeV, are used in the radiotherapy departments of most large

*Corresponding author. CERN, Geneva 23, Switzerland.
[1] Also at University of Milano Bicocca.

0168-9002/$ - see front matter
doi:10.1016/j.nima.2003.07.062

hospitals. This corresponds to about half of the accelerators operated around the world (data by Waldemar H. Scharf and collaborators quoted in Ref. [1]). For comparison, only 25 cyclotrons or synchrotrons are used for tumour treatment with protons and/or carbon ions, an irradiation modality now known as 'hadrontherapy'.

This technique has greatly developed in the last 10 years although the first steps were taken more than 50 years ago. In 1946, at Berkeley, Robert (Bob) Wilson [2] remarked that the narrow Bragg peak characterising the energy loss of a monoenergetic beam of protons, or of other fully stripped light ions, allowed millimetric accuracy in the delivery of a high dose to a tumour target while sparing the surrounding healthy tissues.

To obtain a range of 25 cm in soft tissues, the kinetic energy of the protons has to be 190 MeV, while for carbon ions—at present the second most used charged hadrons—one needs 4500 MeV, i.e. 375 MeV/nucleon.

Since the Bragg peak of monoenergetic particle beams is narrow, for irradiation of thick targets the energy of the charged particles has to be modulated in time, either by an absorber of variable thickness or by varying the energy of the beam delivered by the accelerator (Fig. 1). With a *Spread Out Bragg Peak* (SOBP) of 8–10 cm, the distal fall-off of the proton irradiation dose takes place in 2–3 mm and the dose at the tumour's incident surface is typically 70% of the peak dose. This dose distribution is much more favourable for therapy than the one of high-energy photons, which are characterised by a roughly exponential absorption in matter.

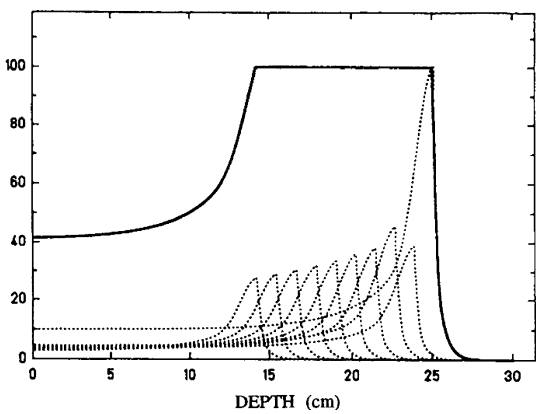

Fig. 1. Schematic drawing of the superposition of many Bragg peaks to produce a flat Spread Out Bragg Peak (SOBP).

Due to the convenient *macroscopic* energy distribution, a truly 'conformal' therapy can be performed with only one or two directions of incidence of the charged hadron beam. Moreover the total energy delivered to the surrounding healthy tissues is definitely lower than the one given even in the most recent forms of photon radiotherapy based on the use of 6–12 crossed beams (Fig. 2).

Since in radiotherapy the main limiting factor is constituted by the dose absorbed in the healthy tissues surrounding the tumour, the physical advantages following from the above-mentioned Bragg peak behaviour are clear. The importance of these physical advantages depends upon the type, localisation and dimensions of the tumour target and it is certainly evident in the case of large tumours, close to critical organs, that cannot be irradiated without influencing the quality of life of the patient.

A global count indicates that by the end of 2002 about 33 000 patients had been treated with proton beams and about 1400 with carbon ions [4]. Protons, having practically the same biological effects as photons, are used because of the superior dose conformation. Carbon ions, however, are better suited than protons (and photons) for the treatment of *radioresistant* tumours, i.e. the slowly growing (mainly hypoxic) tumours that are insensitive to *both* X-rays and protons and represent about 20% of all tumours today treated with X-rays [5]. In particular circumstances also other (light) ions may have specific advantages [6]. Since the Radiobiological Effectiveness (RBE) of the ions increases towards the end of the range in matter, for a uniform clinical dose the physical dose is not flat, as in Fig. 1, but has to decrease with the depth in the SOBP.

At the end of 2002, deep-seated tumours were treated with *protons* in five hospital-based centres, which have several treatment rooms and are fully dedicated to radiation therapy: the Loma Linda University Centre in California, the Northeastern Proton Therapy Centre in Boston, and the three centres in Kashiwa, Tsukuba, and Wasaka Bay

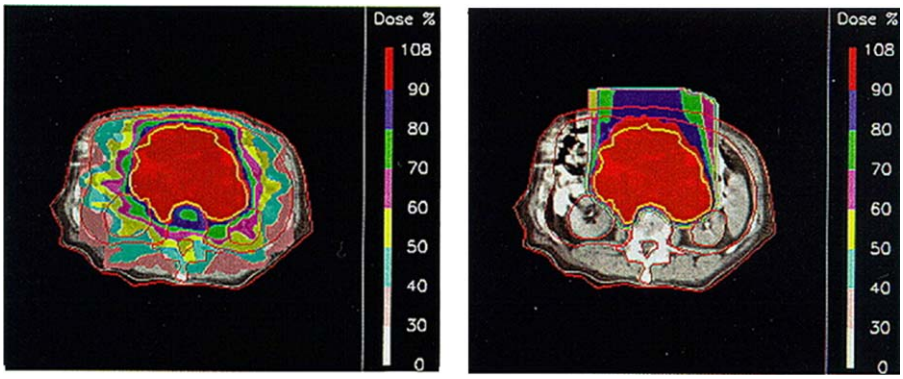

Fig. 2. Treatment plans of a large tumour obtained in an intensity modulated radiation therapy (IMRT) with nine X-ray beams (left) and in protontherapy with one beam (right) [3].

in Japan. Two hospital-based *ion* centres existed in Japan: HIMAC in Chiba and HARIMAC in Hyogo. Many new protontherapy centres were under construction: one in Switzerland, one in Japan, one in Germany, one in Korea, two in China and three in USA. Each of these hospital-based centres can treat 500–1500 patients/year, each patient coming for an average number of 20 sessions for proton irradiations and about 10 sessions for carbon irradiations. A typical session lasts 30 min. All the hospital-based protontherapy centres feature one or more rotating 'gantries' that support magnetic channels allowing irradiation of a lying patient from any angle. Proton gantries can weigh 50–100 ton and have diameters between 8 and 10 m.

In 2002, all the hospital-based centres still use 'passive' dose distribution systems, in which the proton beam is scattered in an absorber and then shaped to the required profile in space using other absorbers and collimators. 'Active' systems are used since a few years in institutes like PSI, Switzerland and GSI, Germany. At PSI, a compact gantry and a 'spot scanning' system for *protons* has been constructed [7], while the *carbon beam* of the GSI synchrotron is equipped to irradiate patients with a horizontal 'raster scanned' pencil beam [8]. In the future, all facilities will be equipped with active dose distribution systems.

Thus, more than 50 years after the first proposal, protontherapy is booming [9]. Four companies offer turn-key systems (based on a normal cyclotron, a superconducting cyclotron and two synchrotrons, respectively). Cyclotrons produce proton beams of fixed energy and the energy variation is obtained by introducing absorbers in a suitable magnetic channel. Synchrotrons, more conveniently, produce beams of which the energy can be varied within the range of required values and can be used to accelerate protons to the energies needed for deep-seated tumours. At the end of 2002, two carbon ions centres were under construction in Europe: the first one is in Heidelberg (Germany) and was designed by GSI, and the second one, designed by TERA, is sited in Pavia (Italy).

2. The 3 GHz proton linac

In 1993, one of us (U.A.) initiated the study of a novel *proton* linear accelerator based on the *same high radio frequency* ($f = 3$ GHz) as used by thousands of *electron* accelerators running in hospitals all over the world. This high frequency implies a linac more compact and shorter than the standard lower-frequency proton linacs, used as injector of most synchrotrons, since the permissible accelerating field is roughly proportional to $f^{1/2}$ [10]. The small iris of a linac of such a high frequency is not a limitation, since the current needed for protontherapy is very small (nanoamperes). Note that a different proposal based on a

lower frequency ($f = 1.3$ GHz) was presented at the LINAC92 conference [11], but was not pursued further.

2.1. The design study

In 1993, the problem of designing a 3 GHz proton linac was tackled in the general framework of a study of novel, so-called 'compact accelerators', initiated by the TERA Foundation and lead by Picardi (ENEA, Frascati, Italy). These studies were concentrated on four different types of accelerators: a compact conventional synchrotron, a high-field synchrotron, a superconducting cyclotron and a 3 GHz linac. The results are described in the '*Green Book*' [12], and some important parameters of the 'linac solution' (Ref. [12, Chapter 9]) are listed in Table 1.

The first design of a 200 MeV, 3 GHz linac has been produced by two of us (K.C. and M.W.) [13], based on beam dynamics programs written by one of us (K.C.). This linac design consisted of a sequence of three accelerators, a *radio frequency quadrupole*, *RFQ* (best ion accelerator at low energies), followed by a novel structure called *side-coupled drift tube linac*, *SCDTL* (L. Picardi et al., patented by ENEA, Ref. [14]), and terminated with a *side-coupled linac*, *SCL* (developed at LANL, USA [15]).

The beam is extracted from the ion source at 80 keV and transported to the RFQ via the low-energy beam transport system. At such a low input energy, the RFQ has to operate at a sub-harmonic of 3 GHz, i.e. at 750 MHz. The RFQ output of 5 MeV is sufficient for the SCDTL to operate at 3 GHz, and to accelerate the beam to 70 MeV. The last accelerator in the chain, the 3 GHz SCL, finally brings the beam to an energy of 200 MeV. Table 2 lists the components of the RF system.

It should be mentioned that it is an unusual feature for an SCDTL as well as for an SCL to operate at 3 GHz for such low proton energies. The advantages of the linac solution are:

(i) the output energy is variable like it is for synchrotrons;
(ii) the time structure is very well suited for application of the spot scanning technique as developed at PSI in Switzerland;
(iii) the transverse beam emittances are about ten times smaller than the typical emittances of cyclotrons and synchrotrons, requiring much smaller gaps in the dipole magnets of the gantry, thus reducing considerably their weight and cost.

Table 1
Parameters of the TERA proton linac

Output energy	70–200 MeV
Average current	20 nA
Beam pulse duration	3 μs
Repetition rate	200 Hz
Beam duty cycle	0.06%
Proton Source and LEBT	
Energy	80 keV
Current	up to 1 mA
Pulse duration	50 μs
Repetition rate	200 Hz
Beam duty cycle	1%
1. RFQ (750 MHz)	
Output energy	5 MeV
Beam peak current	33 μA
Transverse emittance (normalised)	0.2π mm mrad
Longitudinal emittance	0.15π deg MeV
Structure length	2.6 m
RF peak power	600 kW
RF duty cycle	0.1%
2. SCDTL (3 GHz)	
Output energy	70 MeV
Beam peak current	33 μA
Transverse emittance (normalised)	0.2π mm mrad
Longitudinal emittance	0.6π deg MeV
Energy spread, bunch length ($\Delta E, \Delta\varphi$)	0.13 MeV, 4.4°
Structure length	11 m
Number of tanks	56
Number of permanent magnet quads	56
RF peak power	9 MW
RF duty cycle	0.06%
3. SCL (3 GHz)	
Output energy	70–200 MeV
Output peak current	33 μA
Transverse emittance (normalised)	$<0.25\pi$ mm mrad
Longitudinal emittance	0.6π deg MeV
Synchronous phase angle (°)	−13
Energy spread, bunch length ($\Delta E, \Delta\varphi$)	0.2 MeV, 3°
Structure length	11 m
Number of tanks	24
Number of permanent magnet quads	24
RF peak power	30 MW
RF duty cycle	0.06%

It was clear from the beginning that the SCL linac described in Table 1 can also be used downstream of a cyclotron, to boost the low energy of the beam delivered by a standard commercial cyclotron (about 60 MeV) to 200 MeV or more, as needed for deep protontherapy. To such a linac one gave the name LIBO, for LInac BOoster. This has been the focus of our work over the past 6 years.

2.2. The linac of the TOP project

Following the study presented in Chapter 9 of Ref. [12, pp. 215–256], the construction of a 3 GHz proton linac was considered in the framework of activities of the project TOP ('*Terapia Oncologica con Protoni*') of the Istituto Superiore di Sanità in Rome [14]. In order to construct a prototype of the first module of the SCDTL section, a collaboration was set up between ENEA (L. Picardi et al.), Istituto Superiore di Sanità, Rome (M. Grandolfo et al.), and the Oncological Institute Regina Elena, Rome (M. Benassi et al.).

The LIBO studied by TERA and described in this paper, could also be used for the high-energy section of the TOP project.

Table 2
Components of the radiofrequency system

Number of klystrons at 750 MHz	1
Number of klystrons at 3 GHz	13
Total klystron RF peak power	40 MW
Klystron efficiency (%)	40%
Modulator average power	60 kW
DC power for klystron focusing coils	35 kW
Mains power for RF	~120 kW

3. The first design of LIBO

As mentioned above, a 60–200 MeV SCL linac has a wide range of applications, since it opens the possibility to transform a cyclotron (which is useful for eye therapy, isotope production and low-energy physics research) into a 200 MeV accelerator for the treatment of deep-seated tumours. An artist's view of LIBO is shown in Fig. 3.

A 3 GHz LIBO would have a duty cycle of the order of 0.1–0.2%, corresponding to a repetition rate of 200–400 Hz and a pulse duration of 3–5 μs. The cyclotron frequencies are much lower, usually about 25 MHz. Nevertheless, the combination cyclotron–linac can operate for protontherapy, because—as already mentioned—the average beam current needed is small (nanoamperes)

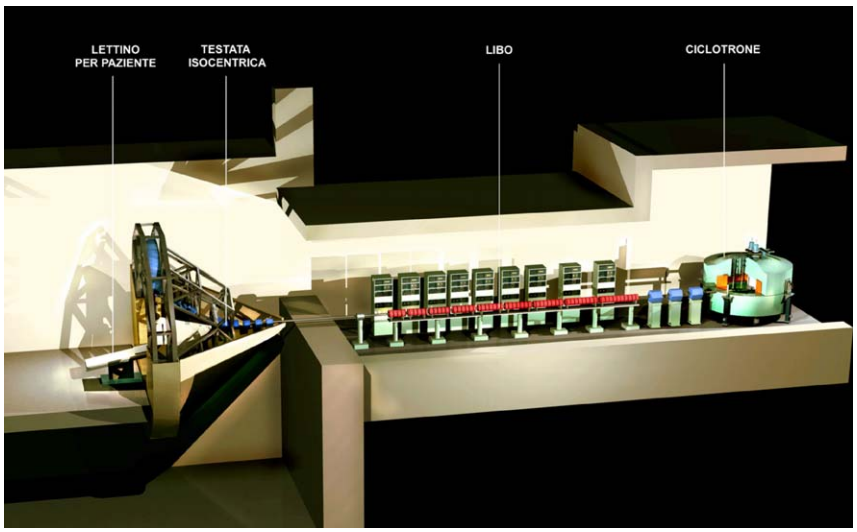

Fig. 3. Artist's view of LIBO with the cyclotron and a rotating gantry.

compared to the current accelerated by a cyclotron (microamperes).

The cyclotron bunches (typically at MHz) will extend over many 3 GHz linac buckets and only the current inside the buckets will be accelerated, while the particles between buckets will eventually be lost. To reduce beam losses and radiation damage in LIBO, the cyclotron source has to be pulsed at the linac repetition rate (e.g. 200–400 Hz), with a pulse duration exceeding the linac pulse.

Due to the particular interest of the Clatterbridge Centre for Oncology in UK (where in 1992 a 1.3 GHz proton linac was considered as a booster for the 62 MeV cyclotron [11]), the first LIBO studies have been based on specifications of the Clatterbridge cyclotron [16]. The first design of beam optics for LIBO is presented in Ref. [12, Chapter 9, Section 12] ('Eye treatment facility and booster options'). A certain number of modifications had to be made to the original parameter list in Table 1 in order to adequately handle the cyclotron beam.

3.1. Transverse and longitudinal acceptances of LIBO

The transverse cyclotron beam emittance is much larger than that of the SCDTL. The normalised transverse cyclotron emittance has been estimated to be 3.7π mm mrad (unnormalised about 10π mm mrad), while the normalised acceptance A_n of the SCL of Table 1 is

$$A_n = \frac{a^2}{\beta^+}\pi\beta\gamma = 1.73\pi \text{ mm mrad}$$

with a representing the aperture radius (3 mm), β^+ the Twiss parameter (1.9 m) and $\beta\gamma$ the relativistic factors (0.365). Evidently, A_n is too small to match the cyclotron emittance. It can, however, be increased either by increasing a or decreasing β^+. Increasing a requires more RF power and results in bigger output emittances in all three phase planes; decreasing β^+ requires a shorter distance between focussing elements, leading to shorter tanks and hence a larger number of them. Several combinations of a and β^+ values have been analysed by two of us (K.C. and M.W.) and the most interesting one was retained for the LIBO design of Ref. [12]. In brief, a has been increased from 3 to 4 mm, and the tanks have been shortened from 17 accelerating cells to only 13, resulting in a normalised transverse acceptance $A_n = 4.2\pi$ mm mrad, large enough to contain the cyclotron beam emittance.

Longitudinally, the synchronous phase angle φ_s of Table 1 was increased from -13 to -19, increasing thus the bucket length ($\sim 3|\varphi_s|$) and the capture efficiency. For simplicity, no attempt was made to match the beam using a buncher. The trapped cyclotron beam resulted to be about 10%. With a *beam duty cycle* of 0.0018 (400 Hz and 4.5 μs) the LIBO trapping efficiency is 1.8×10^{-4}. Hence, in order to get an average output current of 5 nA, which is more than what is needed for deep protontherapy, the peak intensity in the cyclotron beam pulse should be about 30 μA.

3.2. LIBO-62

The LIBO based on the Clatterbridge cyclotron was further studied under the name of LIBO-62. A schematic layout of LIBO-62 is shown in Fig. 4. It is about 13.5 m long and contains 36 *tanks* grouped into nine *modules*. All modules are essentially identical, except for their progressive increase in length, corresponding to the increase of the velocity of protons, from $\beta = 0.35$ to 0.56.

Three elements are at the basis of the accelerating structure: the *half-cell-plate*, the *bridge coupler* and the *end cell*. Each module contains 102 half-cell-plates, three bridge couplers and two end cells. The main computed parameters of the LIBO of Fig. 4 are presented in Table 3.

A permanent magnet quadrupole (PMQ) is inserted between each of the 36 tanks of LIBO-62. Four tanks are grouped into a module, constituting an RF unit, fed by its own RF chain and klystron. Such a solution certainly requires many klystrons, but also permits great flexibility. In particular, it allows to reduce or switch off the power in some modules, thus varying continuously the output beam energy, in accordance with the tumour treatment requirements. The high repetition rate (400 Hz) is needed to enable

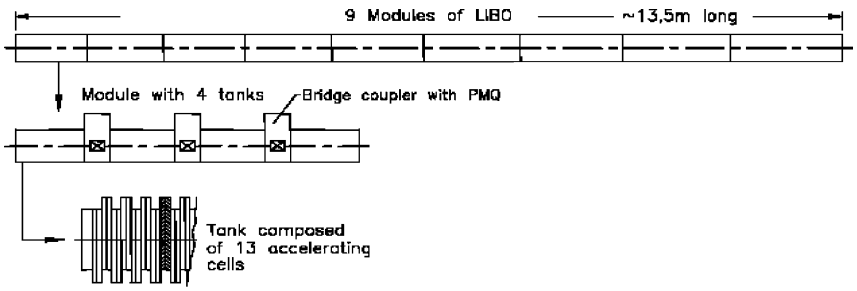

Fig. 4. Schematic layout of LIBO-62.

Table 3
Parameters of the booster linac LIBO-62

Input energy (MeV)	62
Maximum output energy (MeV)	200
Aperture radius (mm)	4
Number of cells/tank	13
Number of tanks/module	4
Number of modules	9
Total number of tanks	36
Number of klystrons	9
Total number of tanks	36
Number of PMQs	36
Total length (m)	13.50
Synchronous phase angle (deg)	−19
Peak RF power (MW)	33
RF duty factor (%)	0.20
Beam duty cycle (%)	0.18
Repetition rate (Hz)	400
Transverse normalised acceptance (π mm mrad)	4.2
Trapped cyclotron beam in (200 ± 1) MeV (%)	13

application of the 'spot scanning' technique, as introduced by PSI, with dose depositions separated by 2.5 ms.

A high accelerating gradient E_0 (equal to 15.8 MV/m averaged over a tank) was selected in order to limit the accelerator length. Care was also taken to avoid synchro-betatron parametric resonances. Beam simulation through the accelerator showed where the particles got lost and what the energy composition of the output beam was. Fig. 5 shows the computed energy distribution of the output beam (200 MeV): 13% of the protons injected by the cyclotron during the LIBO RF pulse are accelerated and come out inside the *energy window* (200 ± 1) MeV.

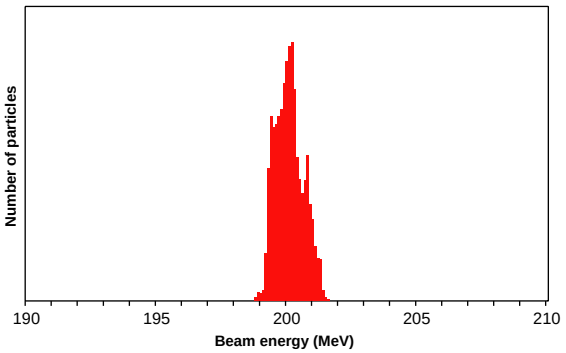

Fig. 5. Output energy distribution of LIBO-62.

3.3. Error analysis of LIBO-62

When optimising an accelerator, the influence of various errors must be taken into account. The beam transmission of 13% was computed for an ideally aligned setup. However, misalignments of PMQs and linac tanks and other errors, such as accelerating field or quadrupole gradient errors, reduce the output intensity of the accelerated beam. The effect of some of these errors was estimated with Monte Carlo optics calculations [17]. Four types of errors have been analysed: quadrupole displacement errors of ±0.1 mm, tank displacement errors of ±0.1 mm, quadrupole rotation errors of ±1° and quadrupole strength errors of ±1%. The only errors that produced a significant reduction in the transmission were the quadrupole displacements. The computations show that with random displacement errors within ±0.1 mm, there is a 90% probability that the transmission will be greater than 10%.

Studies have been made of the effects of both the accelerating cell diameter D and the so-called *web thickness* w (i.e. the wall between two accelerating cells) on the effective shunt impedance per unit length ZT^2 and the peak surface field E_{peak} [17]. The effect of a *coupling slot* for a 3% coupling between accelerating and coupling cells has been included into the evaluation of the shunt impedance. The upper curve in Fig. 6 shows that at the high-energy end of LIBO-62 ($\beta = 0.56$), the chosen diameter D of 70 mm is optimum for ZT^2. The lower curve of Fig. 6 shows that at the low-energy end ($\beta = 0.35$) there is little to be gained in ZT^2 by reducing D and that E_{peak} would increase rapidly. With $D = 70$ mm, E_{peak} is limited to a conservative value of 1.6 times the Kilpatrick limit E_{k}.

Fig. 7 shows that a thin web thickness w is preferable, as one might expect from the short cell lengths in LIBO. A 4 mm web was finally chosen for good mechanical rigidity of the pieces during machining.

The effects of the coupling slots between cells were studied with the 3D program MAFIA. The PSPICE program, dealing with coupled circuits, was used to assess the importance of various errors in the presence of incompletely closed stop bands.

Cold RF measurements on a few cells of an aluminium model having the shape shown in Fig. 8 completed the studies of LIBO-62.

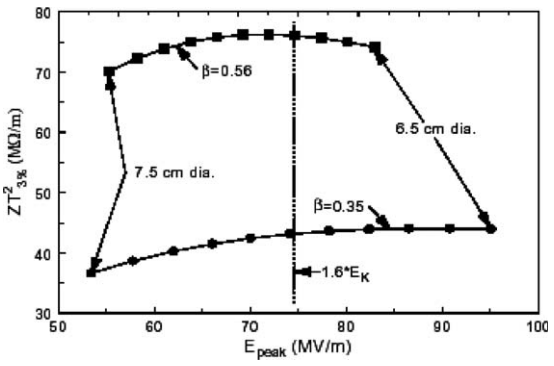

Fig. 6. Shunt impedances and peak surface fields for 11 different cell diameters D, at the LIBO input ($\beta = 0.35$) and output ($\beta = 0.56$) energies. The web thickness w is 4 mm.

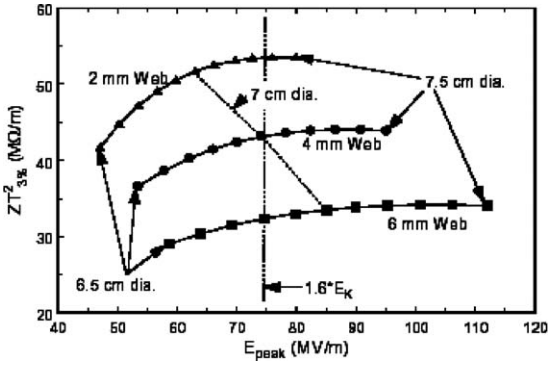

Fig. 7. Shunt impedances and peak surface fields for 11 different cell diameters D and three web thicknesses w, at the input energy ($\beta = 0.35$).

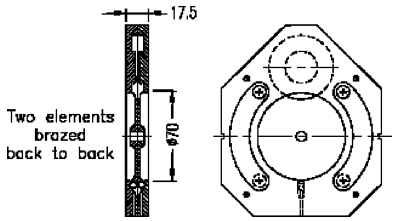

Fig. 8. Shape of the aluminium cells used for the first RF measurements.

3.4. Cooling of LIBO-62

One of the really delicate issues is the question whether cooling channels are required inside the web or whether an external, circumferential cooling alone is sufficient. Cooling channels inside the web would necessitate a relatively thick web, which would spoil the electrical characteristics and complicate the mechanical design, thus adding extra risks and costs.

The cooling problem was studied assuming an RF duty factor of 0.2%, for which about 150 W are dissipated in each accelerating cell of the first tank [17]. (Note that very little power is dissipated in the coupling cells because LIBO operates in the $\pi/2$ mode.) The value of the power dissipated on the walls of the accelerating cells, as computed by SUPERFISH, was used as an input for the finite element engineering code ANSYS. External cooling was simulated with the simplifying assumption of a constant and uniform sink temperature, T_{sink},

at a predetermined radial distance r from the accelerating cell axis. It was found that the temperature gradient between the accelerating cell centre ('nose') and T_{sink} ('ambient temperature') at $r = 45$ mm is typically 7°C.

A program was written especially for the purpose of computing the resonance frequency of the cells distorted as a consequence of this temperature gradient. The code reads the coordinates of the deformed cell surface from ANSYS, compares them with the original values and computes the frequency detuning Δf. The detuning Δf was found to be about -250 kHz, if T_{sink} was held at its ambient value. Decreasing T_{sink} deforms the cells in the opposite sense. It was found that changing T_{sink} by -5°C restores the original resonance frequency of the cells (Fig. 9).

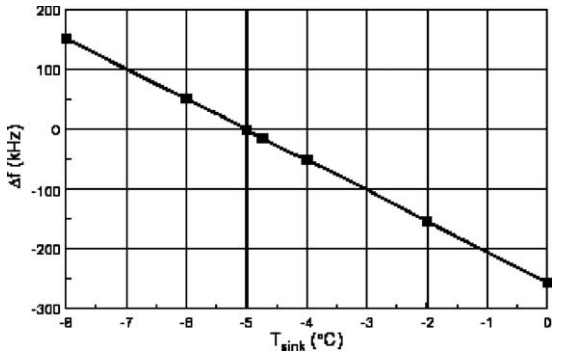

Fig. 9. Detuning Δf as function of the change of the sink temperature T_{sink}.

The conclusion is that external cooling is adequate for LIBO and that, by controlling T_{sink} with a frequency feedback loop, it will be possible to keep the accelerator on tune.

4. The LIBO prototype

At the end of 1998, it was decided to build and test a prototype of LIBO-62. For that, the first module, the most critical one, that has to accelerate protons from 62 to 74 MeV, was chosen. It requires an RF peak power of about 4.4 MW, at 2.998 GHz. The construction of this 'prototype module' was completed in 2000, after which full RF power tests were performed at CERN. Fig. 10 represents this LIBO prototype. Details of construction and tests are also given in Refs. [18,19].

Among the basic elements that constitute a module (see Section 3.2), by far the most numerous one is the half-cell plate. It is the basic building block of a tank, being in fact a rectangular plate containing half of an accelerating cell and, on the reverse side, half of a coupling cell (Fig. 11). The shape of the cells has been studied using the programs SUPERFISH and MAFIA.

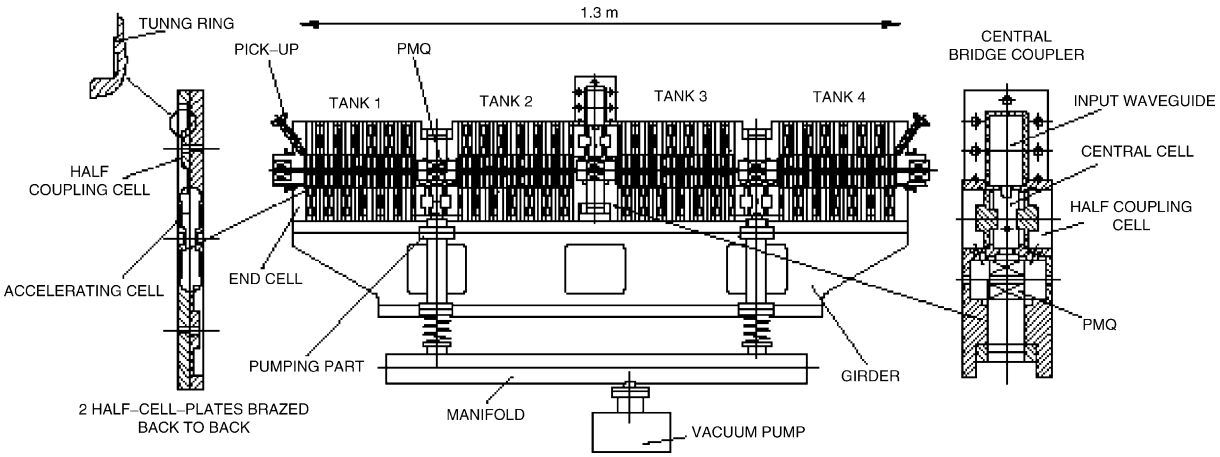

Fig. 10. Layout of the LIBO prototype.

The tanks of a module are resonantly coupled via three bridge couplers, each formed of three cells. The central coupler is connected to the RF feeder line, by which the RF power is supplied to the module. The remaining two couplers are connected to the vacuum system. RF pick-up loops are installed at either end of a tank (in the bridge couplers and the end cells). The PMQs, placed between the tanks, form a FODO focussing lattice (Figs. 10 and 12). The bridge couplers and the end cells are equipped with movable tuners for frequency correction after the module has been brazed into one piece. Such a tuning nevertheless requires to break the vacuum in the accelerator.

Fig. 11. Half-cell plates showing a coupling half-cell (left) and an accelerating half-cell (right). Note the coupling slot.

The bridge couplers and the end cells have stainless-steel flanges into which cylindrical inserts are brazed in order to enable fixation of the module onto a rigid girder, minimising the risk of stress and deformation in the soft copper. The girder is equipped with fixed external reference marks for alignment purposes. Also the connections to the beam line at both ends of the module and the pumping ports to the vacuum manifold are in stainless steel.

4.1. Material and brazing

The basic half-cell plates, each containing an accelerating half-cell and a coupling half-cell, are made of laminated OFE copper. The cells within a specific tank have all the same dimensions. Bridge couplers and end cells are made of forged OFE copper and equipped with brazed 316 LN stainless-steel flanges for vacuum openings,

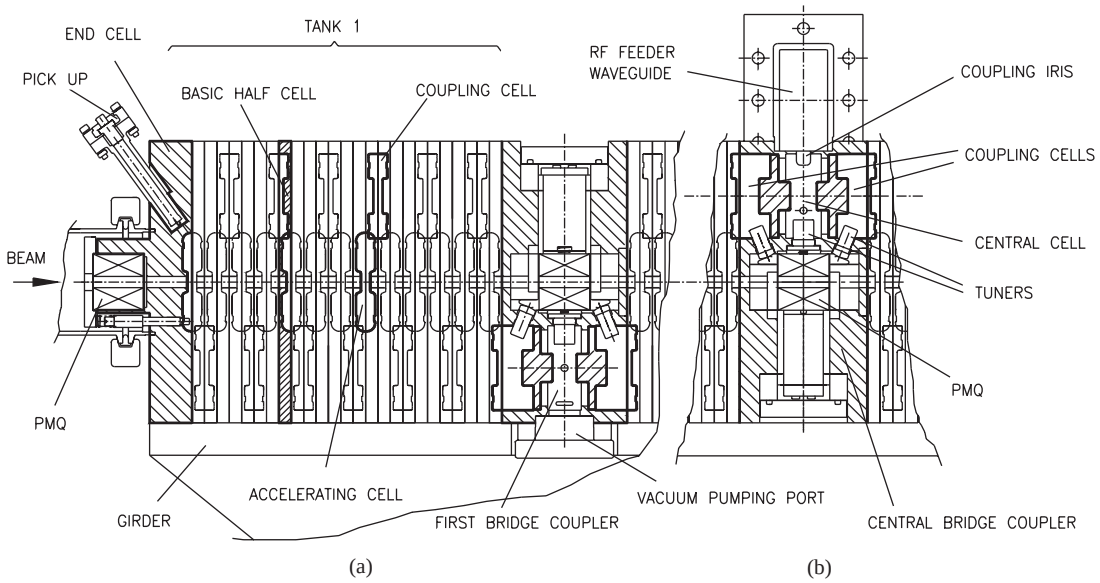

Fig. 12. Partial drawing of the prototype: (a) first tank with end cell and one of the lateral bridge couplers; (b) central bridge coupler with the RF feeder waveguide and the permanent quadrupole (PMQ).

RF pick-ups, and fixation slugs. All the elements have been machined at CERN on CNC lathes and milling machines. The pre-machined basic half-cell plates were stress-relieved in air at 250°C in order to guarantee, after a final machining operation, the 20 μm planarity required for vacuum brazing of the structure.

Special attention has been paid to the mechanical precision of the coupling slot between the accelerating and coupling half cells. Its length, constant over the whole prototype, was precisely machined by milling to better than 0.1 mm.

Prior to brazing all elements were thoroughly cleaned. Insertion of the brazing alloy as well as the stepwise assembly was done inside a clean room under laminar air flow. Brazing was done in an all-metal vacuum oven and at four temperatures, ranging (and decreasing) from 850°C to 750°C. Two methods have been applied for the application of the brazing material: standard silver-based alloys in the form of *wires* positioned in pre-machined grooves, and in the form of *foils*. The components of the module were brazed in seven separate subassemblies—four tanks and three bridge couplers—that were then piled up vertically in the oven for the last two brazing steps. Fig. 13 shows the LIBO module placed vertically in the oven; as a consequence the brazing surfaces are horizontal, with brazing grooves facing down.

The lateral tuning rods in the accelerating and coupling cells (see Section 5), cut to the right length, were fixed in position and blocked with ceramic pieces and molybdenum springs during brazing. After the last brazing step, concerning the cooling plates, the module was fixed onto a rigid girder to guarantee stiffness during further manipulations. Leak detection after brazing was followed by a vacuum test of the fully equipped module. Vacuum levels of 5×10^{-7} and 5×10^{-8} mbar were reached in the module prototype and in the vacuum manifold respectively. This is much better than the design requirement of 10^{-6} mbar.

After the final brazing, a 3D metrology measurement with a basic accuracy of ± 3 μm was performed. The results showed that each of the PMQ axes is within a transverse distance of <0.1 mm from the ideal accelerator axis, as required by beam dynamics specifications.

Fig. 13. The module placed vertically in the oven.

4.2. Cooling plates

The cooling of the LIBO module is provided by demineralised water flowing through channels inside specially designed copper plates. Each tank has two cooling plates, brazed to two opposite sides. For a module, this amounts to a total of eight parallel circuits with a total water flow of 200 l/min. Apart from simplifying the cooling scheme, the use of these (external) plates also avoids the risk of water leaks inside the accelerating structure. A transfer forced convection coefficient of 14 000 W/(m^2 C) for each circuit assures the cooling of the LIBO tank when operated at a full average power of 2.2 kW. If facilities are available to vary the water temperature, the 'cooling' plates can be used as a tool for fine-tuning of the cavity, see Section 6.

5. RF aspects

The design of LIBO is based on a mean accelerating field value E_0 on axis which is identical in all the tanks. To achieve this in the prototype, the accelerating cells increase in length from tank to tank (conforming to the increasing velocity of protons), while the dimensions of the coupling cells and of the coupling slots in all the half-cell plates of the module do not vary. As consequence, the corresponding coupling coefficient ($\cong$4.3%) decreases $\propto \beta^{-1/2}$, as required to have $E_0 = \text{const}$.

The bridge couplers between the tanks are of the three-cell magnetically coupled type. The two coupling cells in the bridge coupler are longer than in the tanks, thus providing sufficient space to house the PMQ (Fig. 12). The central cell ('accelerating') of the central bridge coupler has an iris to connect it to the waveguide that brings the RF power to the module. The waveguide is connected tangentially to the central cell (Fig. 10) and is terminated by a short-circuit at a distance of $5\lambda/4$ from the iris.

5.1. Tuning during production

The resonance frequency adjustment procedure made use of three tuning tools: tuning rings, tuning rods and screw tuners. The tuning rings and rods were available in each half-cell, while the variable screw tuners equipped the end cells and the bridge couplers. Each tool was used at a given stage of the prototype production.

The tuning of the cells was done in parallel with the production, in a series of steps. Each half-cell in the tank has a 0.7 mm high and 2 mm wide tuning ring on the flat face (Fig. 10). After RF measurements, the remachining of the ring can bring the individual half-cell resonance frequency within 0.5 MHz with respect to the nominal value. The sensitivity of the frequency is about 1.5 MHz per 0.1 mm of the ring height and so the tuning is achievable with conventional machine tolerances.

5.2. RF measurements on basic cells and tanks

The main problem of the RF measurements of cells *before* brazing are the low Q-values which stem from ill-defined RF contacts over large surfaces.

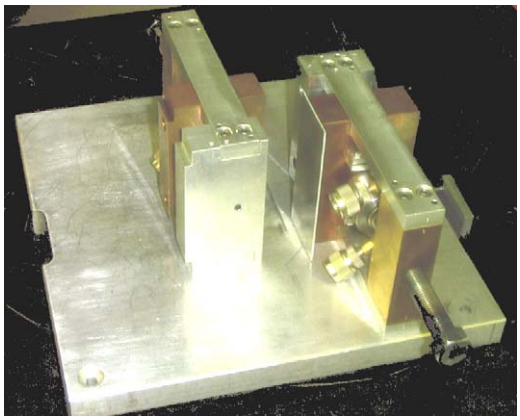

Fig. 14. Tool for RF measurement on basic cells.

Special tools have been designed and built to improve the situation (Fig. 14), and typical Q-values of about 2000 (to be compared to the computed value of 7500) have been obtained in single half-cell measurements. The Q-value of an unbrazed tank was typically as low as 700, which was one of the main reasons for the resonance frequency changes observed after the brazing.

After the brazing of all individual tanks of the prototype (tanks 1 and 4 equipped with their end cells), they have been aligned on a marble table for RF measurements (Fig. 15).

In order to compensate for residual frequency errors due to the brazing of the cells and to enable tuning of the complete module to the correct operational frequency, each (coupling and accelerating) half-cell has a lateral hole into which a small tuning rod is inserted. These rods have been adjusted to the correct length and then brazed during the before-last brazing step.

5.3. Tuning of the bridge coupler

For the tuning of the three-cell magnetically coupled bridge couplers, neither tuning rods nor rings were used. Once finished, the bridges were tuned with adjustable screw tuners, a facility that, in contrast to the tuning rods, could be employed also *after* the final brazing (Fig. 12).

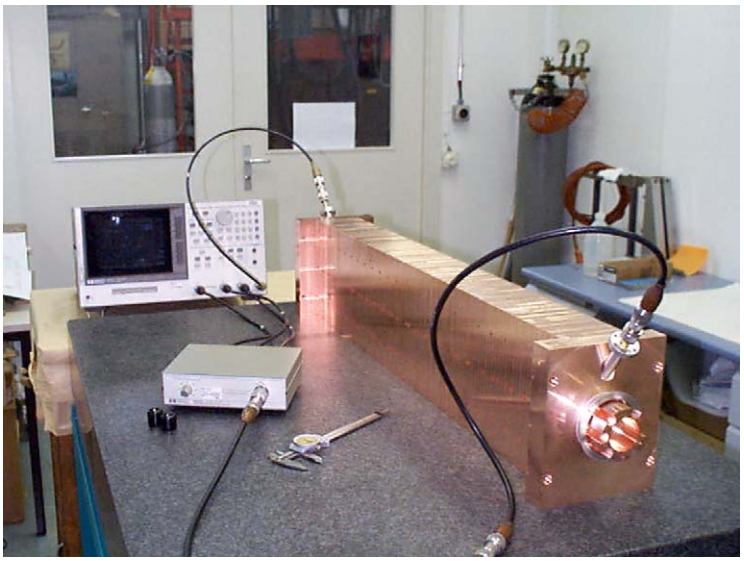

Fig. 15. RF measurement set-up.

The tuning procedure is based on the fact that, for a coupled resonator system, the only direct measurable quantities are the resonant frequencies of the whole structure, which differ from the single cell values. Assume that for a three-coupled-cell system like the three-cell bridge, the unknown single-cell frequencies are ω_1, ω_2 and ω_3, while the frequencies which can be measured are ω_-, $\bar{\omega}$ and ω_+, corresponding to the 0, $\pi/2$ and π modes, respectively. The tuning procedure consists, first, in *equalising* the frequencies of the coupling cells of the bridge using tuning screws ($\omega_1 = \omega_3$) and then *varying*, with a tuning screw, the central cell frequency ω_2 to get a set of measured data. For $\omega_1 = \omega_3$, a linear relation applies between some combinations of the measured frequencies [20]

$$\frac{\bar{\omega}^2}{\omega_+^2} + \frac{\bar{\omega}^2}{\omega_-^2} = \frac{1 - k_2/2}{1 + k_2/2} + \frac{\bar{\omega}^4}{\omega_+^2 \omega_-^2} \frac{1 + k_2/2}{1 - k_2/2 - k_1^2/2}.$$

By a linear fit to the data using the above formula, it is possible to derive the first and second coupling coefficients, k_1 and k_2 (first and second nearest-neighbour coupling), and then obtain the single-cell frequencies from the theory of coupled resonant cavities. In this way, one could correctly tune the cells in the bridge couplers, except for the central cell of the central bridge, which remained 6.5 MHz below the nominal value due to a machining error. This caused a small bump in the field level between tanks 2 and 3 (Fig. 16).

The waveguide of the RF feeder line was brazed tangentially to the central bridge coupler and was terminated by a short-circuit at $5\lambda/4$ from the centre of the elliptical coupling iris. The approximate dimension of the iris was determined by applying the Slater's tuning curve method to a series of frequency-domain MAFIA simulations [21]. The finally measured coupling factor β of the LIBO to the waveguide was 1.14, corresponding to a reflected input power of 0.4%.

The complete module (tanks and bridge couplers) was assembled and measured in advance of the penultimate brazing, and the length of the tuning rods in the accelerating cells (one per half-cell) was adjusted to give the correct overall frequency and the required field flatness. Acting in the same way on the coupling cells, the stop band was adjusted to be +150 kHz. All the rod tuners in a tank, except in the accelerating cells at the ends, are cut to the same length. In fact they were used essentially to compensate the differences in tank frequencies and to act on the stop band, but not to equalise the single-cell resonance frequencies. No difference was found between the

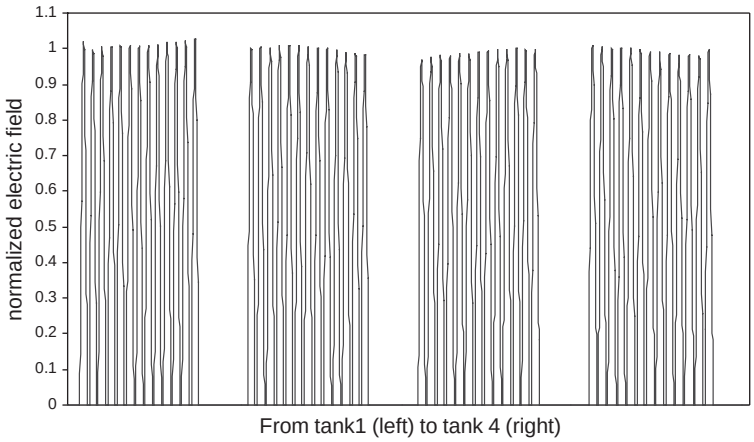

Fig. 16. The acceleration field distribution in the four tanks of LIBO. Deviations from the mean value are less than 3%.

frequency and field distribution measured before and after the vertical (ultimate) brazing, as was verified by bead-pulling measurements (Fig. 16).

6. RF power tests

To adjust the LIBO accelerating field to the correct value during the power tests, the *total shunt impedance* r_s of the module has to be known. This impedance was determined prior to the tests by means of an innovative combination of perturbation measurements and SUPERFISH computations.

As perturbative element a nylon wire was used, stretched along the axis of the whole accelerator. The dielectric constant of the wire had been determined beforehand in a parallelpiped test cavity with a known field distribution. The perturbation with the wire gave the average field amplitude on axis of the whole module, while the electric field distribution was obtained from calculations with the 2D SUPERFISH code. This method avoids the sources of errors encountered when a bead is used as perturbative element: the bead has to be very small because the 3 GHz cells are short, but a small bead makes an insufficient perturbation to the accelerator field. In addition, the new method allows a very rapid evaluation of the total shunt impedance and can be applied to all kind of multi-cell linacs.

The measured value of the total shunt impedance is $r_s = 50\ \mathrm{M\Omega}$, with an estimated error of $\pm 5\%$.

The LIBO prototype module, RF tuned and vacuum tested, was installed at CERN in the LIL area in November 2000, after the operation of LEP has been stopped. It was connected to the vacuum equipment and thermostat-controlled water supply available in this area, and it was powered by a klystron-modulator test system.

Fig. 17 shows the LIBO module installed at LIL: one distinguishes the waveguide of the RF feeder line as well as valves and tubes supplying the water to the channels of the cooling plates. The vacuum manifold with the ion and turbo pumps is mounted underneath the LIBO.

Fine tuning of the frequency during the power tests was done by changing the temperature of the LIBO structure, achieved by adjusting the temperature of the water circulating in the cooling plates. There was no need for feedback loops, because the stability of the water temperature ($\pm 0.1^{\circ}$C) was sufficient to keep the cavity on tune. During the tests the pulse repetition rate was 100 Hz.

The conditioning of LIBO started with a short pulse length of 2 μs. After 72 h of conditioning, the peak RF power $P = 4.4$ MW was exceeded practically without multipactoring and with a very limited number of breakdowns. This power corresponds to the nominal accelerating field level

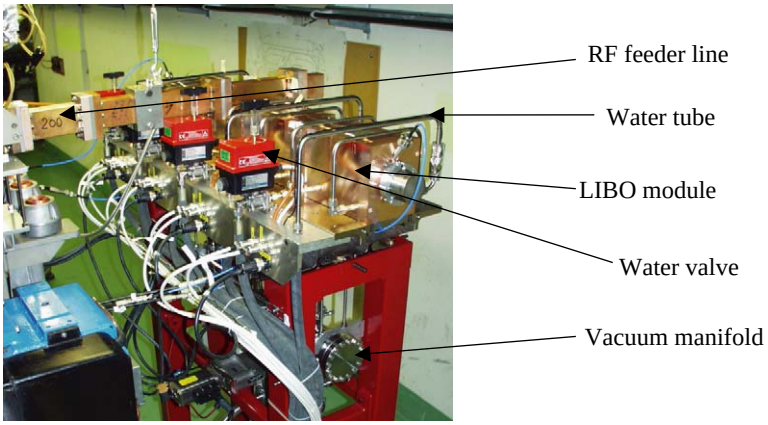

Fig. 17. The LIBO module installed in the LIL tunnel.

in each tank of 15.8 MV/m. Having extended the pulse length to 5 μs, a peak power $P = 14.2$ MW was reached 14 h later corresponding to an accelerating field level of 28.4 MV/m. The computed maximum surface field was 2.6 times the Kilpatrick limit. A further increase of the RF input power was unfortunately prohibited by the power limit of the installed circulator. There were, however, no clear indications that the field level in LIBO could not have been raised further.

The above field level in the module was determined by the input power and the previously measured shunt impedance r_s. Five pick-up loops installed at the input and output of LIBO and in the three bridge couplers allowed the monitoring of the field distribution in the prototype.

To get an independent check of the apparently high field level in the prototype as determined above, the structure temperature was measured as a function of injected power and of water flow. Thermocouples fixed on each tank, and platinum resistive probes mounted on water tubes provided a precise temperature measurement. By varying the water flow for one of the tanks, temperature gradients could be achieved with respect to the three others. The results obtained for different RF power levels were compared with computations: the whole set of measurements was in agreement within the accuracy of the experiment (7%).

A second check consisted in measuring the end point of the Bremsstrahlung X-ray spectra emitted from the cavities. For this measurement we made use of an NaI(Tl) detector. The high level of background allowed, however, only a rough estimate of the field level in the tanks which did not contradict the other measurements.

We strongly believe that the short conditioning time and the very limited number of electrical breakdowns were the result of the great care taken during the design and construction of the prototype: the precision of design and manufacture of the cells, the high surface cleanliness of the structure elements, the accuracy of the brazing operations and the applied RF tuning procedures.

7. Preliminary acceleration tests

In 2001, the LIBO prototype was transported to and installed at the *Laboratorio Nazionale del Sud* (LNS) in Catania to undergo tests with a proton beam. A view of LIBO placed in the beam line of the INFN superconducting cyclotron is shown in Fig. 18. The proton beam delivered by the cyclotron had an energy of (62 ± 0.2) MeV and the operating value of the average current at the LIBO entrance was of the order of 1 nA.

Conventional diagnostic systems like Faraday cups and alumina screens were placed upstream and downstream of LIBO. Moreover, a set of movable thin scintillating fibers developed at LNS [22] was used to control the beam profiles. This system was extremely useful for centring the beam

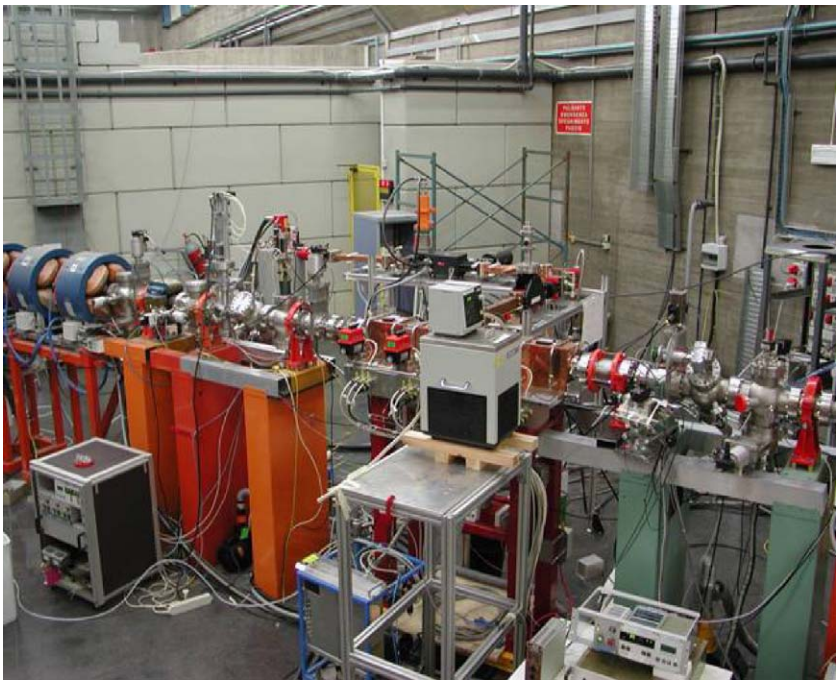

Fig. 18. LIBO installed in the test beam line at LNS of INFN in Catania.

at the very low beam intensities available during the tests.

A very compact solid-state modulator and a 2.998 GHz klystron—lent by the firm IBA (Ion Beam Applications, Belgium) in the framework of a scientific collaboration—was installed and coupled to LIBO. First acceleration tests were performed at the beginning of 2002 [23].

Measurements of the energy of the accelerated protons were done with a 25-mm-thick NaI(Tl) crystal, directly positioned in the beam path. The use of a nuclear detector was mandatory because of the low accelerated beam intensity, resulting from the available cyclotron current and the low duty cycle. The NaI(Tl) crystal was calibrated, in energy resolution and linearity, using the 62 MeV cyclotron beam as a reference.

The cyclotron beam was pulsed at the linac repetition rate (10 Hz) and, because of a time jitter in the chopper, the pulse length was about six times longer than the linac pulse. The number of 62 MeV protons, which were not accelerated in the structure, was so high with respect to the accelerated ones, that the obtained spectra presented an unacceptable background. To remove these unwanted protons, a 30-mm-thick Perspex absorber was placed between the LIBO module and the detector, so that only protons with an energy above 65 MeV could reach the detector.

A typical spectrum of the accelerated proton beam is shown in Fig. 19, where corrections to the energy of the protons for the absorptions in the beam path (Mylar windows, Perspex absorber, air and detector entrance windows) are included.

The peak energy of 73 MeV, corresponding to an energy gain of 11 MeV, was obtained by injecting into the cavity only 3.4 MW (error: $\pm 7\%$) of peak RF power, the maximum that could be delivered during the tests due to limitations in the driver amplifier. As mentioned before, the peak power for a nominal energy gain of 12 MeV and a synchronous phase $\varphi_s = -19$ is $P = 4.4$ MV. The formula linking the power P, the energy gain ΔW and the synchronous phase φ_s is

$$P = \left(\frac{\Delta W}{qT\cos\varphi_s}\right)^2 \frac{1}{r_s}$$

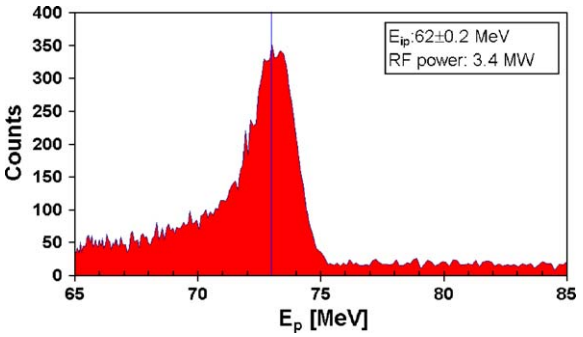

Fig. 19. Energy spectrum of protons accelerated by the LIBO prototype module [23].

where T is the transit time factor, q the proton charge and r_s the total shunt impedance ($= 50\ \mathrm{M\Omega}$). With $P = 3.4$ MW and $\Delta W = 11$ MeV, the spectrum of Fig. 19 corresponds to accelerated protons with $|\varphi| < 5$. These first results prove that the LIBO prototype works in accordance with the predictions.

Further results of the Catania test will be presented in a forthcoming publication.

8. Conclusions and perspectives

A prototype module of LIBO has been built and successfully tested at CERN and LNS, where it has accelerated 62 MeV protons to an energy of 73 MeV, in agreement with the results of the simulations. The working principle of LIBO has thus been fully demonstrated.

The results obtained also strongly indicate that higher accelerating gradients can be applied. For a new design one can aim at an average accelerating field of 20 MeV/m. Moreover, elaborating the construction technique applied for the present LIBO prototype, one can now envisage a reduction of the copper thickness of the cell walls. Thus, without changing the cell design and the construction method, the input energy can be decreased from 62 MeV to 30 MeV, whilst maintaining the goal of 200 MeV at the output. This possibility of a higher gradient (and thus shorter) LIBO starting from a lower energy opens the way to the use of relatively inexpensive commercial cyclotrons as injectors.

Acknowledgements

For the construction at CERN of the LIBO prototype and the RF tests we acknowledge the help of D. Allard, R. Bossart, A. Catinaccio, Ch. Dutriat, J.C. Gervais, S. Haider, D. Leroy, M. Mezin, J. Mourier, M. O'Neil, B. Pincott, Ph. Potdevin, L. Rinolfi, G. Rossat, J. Stovall and G. Yvon. The care of Serge Mathot in the alignment and brazing of the components of the module has been instrumental to the success.

At the PS division of CERN, the RF, PO, PC and PP groups put several pieces of equipment at our disposal, while the vacuum group of LHC supplied the required pumping system.

The installation and acceleration tests at the LNS-INFN profited from the assistance of the staff and personnel of the Catania laboratory. The tests in Catania and the results achieved would not have been possible without the invaluable help of many people: L. Calabretta, V. Campagna, D. Rifuggiato, A. Rovelli, S. Russo and S. Salomone. F. Alessandria, C. Birattari, L. Grilli, from the University of Milan, have given continuous and decisive help since the beginning of the preparations for the tests. A useful support was given by G. Passeggio, R. Rocco and B. D'Aquino of INFN-Napoli for the mechanical drawings and for the machining of bridge coupler prototypes.

The Catania test could not have taken place without the support of Yves Jongen who authorized the lendings of the solid state modulator-klystron system by IBA.

To all these people we express our deepest thanks.

The TERA group is grateful to the Price Foundation (Geneva) and to Compagnia di San Paolo (Torino) for financial support.

References

[1] U. Amaldi, Europhys. News 31 (6) (2000) 5.
[2] R.R. Wilson, Radiology 47 (1946) 487.
[3] A. Zurlo, et al., Int. J. Radiat. Oncol. Biol. Phys. 48 (2000) 277.
[4] J. Sisterson (Ed.), Particles No. 27, January 2003.
[5] G. Kraft, Strahlenther. Onkol. 166 (1990) 10;
G. Kraft, Prog. Part. Nucl. Phys. 45 (2000) 473.

[6] A. Brahme, et al., Nucl. Instr. and Meth. B 184 (2001) 569.
[7] E. Pedroni, et al., Med. Phys. 22 (1) (1995) 250.
[8] Th. Haberer, et al., Nucl. Instr. and Meth. A 330 (1993) 296.
[9] U. Amaldi, Nucl. Phys. Meth. Phys. Res. A 654 (1999) 375c.
[10] W.D. Kilpatrick, Rev. Sci. Instrum. 28 (1957) 824.
[11] M.P.S. Nightingale, A.J.T. Holmes, N. Griffiths, Booster linear accelerator for proton therapy, Proceedings of the Linear Acceleration Conference on LINAC92, Ottawa, 1992, pp. 398–401.
[12] U. Amaldi, M. Grandolfo, L. Picardi (Eds.) The RITA network and the design of compact proton accelerators, INFN-Laboratori Nazionali, Frascati, 1996.
[13] K. Crandall, M. Weiss, Preliminary design of compact linac for TERA, TERA 94/34 ACC 20, September 1994.
[14] L. Picardi, C. Ronsivalle, A. Vignati, Progetto del TOP linac, ENEA, Dip.Innovazione, RT/INN/97/17, 1997.
[15] E.A. Knapp, et al., Rev. Sci. Instrum. 39 (1968) 979.
[16] J.A. Clarke, et al., Assessing the suitability of a medical cyclotron as an injector for an energy upgrade, Proceedings of the European Particle Acceleration Conference on EPAC, Stockholm, 1998, pp. 2374–2376.
[17] U. Amaldi, et al., LIBO—A 3 GHz proton linac booster of 200 MeV for cancer therapy, Proceedings of the Linear Acceleration Conference on LINAC'98, Chicago, 1998, pp. 633–635.
[18] P. Berra, et al., Study, construction and test of a 3 GHz proton linac-booster (LIBO) for cancer therapy, Proceedings of the European Particle Acceleration Conference on EPAC, Wien, 2000, pp. 2495–2497.
[19] B. Szeless, et al., Successful high power test of a proton linac booster (LIBO) prototype for hadrontherapy, Proceedings of the European Particle Acceleration Conference on PAC, Chicago, 2001, pp. 642–644.
[20] D. Davino, et al., A perturbative study of the scattering matrix of a two-port device chain, Proceedings of the ISTET 2001, Linz, August 2001.
[21] J.C. Slater, Microwave Electronics, D. Van Nostrand, New York, 1950, p. 97.
[22] P. Finocchiaro, et al., Nucl. Instr. and Meth. A 385 (1997) 31.
[23] C. De Martinis, et al., Beam tests on a proton linac booster for hadrontherapy, Proceedings of the European Particle Acceleration Conference on EPAC, Paris, 2002, pp. 2727–2729.